PAPER • **OPEN ACCESS**

Serum-derived protein coronas affect nanoparticle interactions with brain cells

OPEN ACCESS
IOP Publishing
Nanotechnology

Nanotechnology **35** (2024) 495101 (15pp)
https://doi.org/10.1088/1361-6528/ad7b40

Serum-derived protein coronas affect nanoparticle interactions with brain cells

Nabila Morshed[1], Claire Rennie[1,*], Wei Deng[2], Lyndsey Collins-Praino[3] and Andrew Care[1,4,*]

[1] School of Life Sciences, University of Technology Sydney, Sydney, NSW 2007, Australia
[2] School of Biomedical Engineering, University of Technology Sydney, Gadigal Country, Sydney, NSW 2007, Australia
[3] School of Biomedicine, Faculty of Health and Medical Sciences, The University of Adelaide, Adelaide, SA 5005, Australia
[4] Biologics Innovation Facility, University of Technology Sydney, Gadigal Country, Sydney, NSW 2007, Australia

E-mail: claire.rennie@uts.edu.au and Andrew.Care@uts.edu.au

Received 4 June 2024, revised 27 August 2024
Accepted for publication 16 September 2024
Published 25 September 2024

Abstract

Neuronanomedicine is an emerging field bridging the gap between neuromedicine and novel nanotherapeutics. Despite promise, clinical translation of neuronanomedicine remains elusive, possibly due to a dearth of information regarding the effect of the protein corona on these neuronanomedicines. The protein corona, a layer of proteins adsorbed to nanoparticles following exposure to biological fluids, ultimately determines the fate of nanoparticles in biological systems, dictating nanoparticle–cell interactions. To date, few studies have investigated the effect of the protein corona on interactions with brain-derived cells, an important consideration for the development of neuronanomedicines. Here, two polymeric nanoparticles, poly(lactic-co-glycolic acid) (PLGA) and PLGA-polyethylene glycol (PLGA-PEG), were used to obtain serum-derived protein coronas. Protein corona characterization and liquid chromatography mass spectrometry analysis revealed distinct differences in biophysical properties and protein composition. PLGA protein coronas contained high abundance of globins (60%) and apolipoproteins (21%), while PLGA-PEG protein coronas contained fewer globins (42%) and high abundance of protease inhibitors (28%). Corona coated PLGA nanoparticles were readily internalized into microglia and neuronal cells, but not into astrocytes. Internalization of nanoparticles was associated with pro-inflammatory cytokine release and decreased neuronal cell viability, however, viability was rescued in cells treated with corona coated nanoparticles. These results showcase the importance of the protein corona in mediating nanoparticle–cell interactions.

Supplementary material for this article is available online

Keywords: protein corona, bio-nano interactions, neuronanomedicine, polymeric nanoparticles, neurons, glia, targeted drug delivery

* Authors to whom any correspondence should be addressed.

1. Introduction

Neuronanomedicine aims to utilize nanoparticle-based drug delivery systems (NDDSs) to enhance therapeutic development for neurological disorders, such as Alzheimer's disease, Parkinson's disease, and brain cancer [1, 2]. NDDSs have the capacity to encapsulate drugs and enhance their solubility, stability, and safety, while also facilitating blood–brain barrier (BBB) crossing and targeted delivery into brain cells [1]. Despite promising preclinical success, however, to date, the clinical translation of neuronanomedicines that are safe and efficacious has remained elusive [1, 3, 4]. This ongoing challenge is partly due to an incomplete understanding of nanoparticle–cell interactions within complex biological environments, particularly the brain, which has critical implications for optimizing the safety and efficacy of NDDSs [4].

One underappreciated player in this process is the potential role of the protein corona. Upon encountering a biological fluid, nanoparticles adsorb fluid proteins onto their surfaces, forming a 'protein corona,' which, in turn, alters their biophysical properties (i.e., size, shape, dispersity, surface functionality) [5]. This phenomenon endows nanoparticles with a new and distinctive 'biological identity', which affects their engagement with biological systems. This includes their interplay with cells (e.g., uptake, cytotoxicity), as well as their overall *in vivo* fate (e.g. immunogenicity, pharmacokinetics, biodistribution, nanotoxicity) [6].

While the protein corona has the capacity to significantly impact the way that NDDSs interact with cells in the brain, with subsequent implications for fine-tuning therapeutic development of these systems, to date, this has remained a largely unexplored aspect of neuronanomedicine. Only a handful of prior *in vitro* studies have investigated the impact of protein coronas on interactions between nanoparticles and brain cells, including uptake, toxicity, and immune responses [3, 7–10]. Further, within this small number of prior studies, there is often a narrow focus on effects on BBB cells (e.g. bEnd.3 endothelial cells) [8, 9], either alone or in combination with only one other brain cell subtype, typically microglia—the brain's immune cells [3, 7, 11]. While this experimental design gives important insights into the brain delivery of NDDS, it overlooks the interplay and potentially distinct biological effects of corona–nanoparticle complexes on the various specialized cell types within the brain parenchyma (i.e., glia, neurons). Additionally, these *in vitro* studies largely lack comprehensive protein corona characterization data, hindering accurate correlation between corona composition and nanoparticle-brain cell associations, which is critical for informing understanding of potential functional effects [3, 7–9].

Motivated by this knowledge gap, we set out to explore how protein coronas influence interactions between nanoparticles and key brain cell types: microglia, astrocytes, and neurons. Herein, polymeric poly(lactic-co-glycolic acid) (PLGA) nanoparticles, with and without polyethylene glycol (PEG) surface coatings (PLGA-PEG), were exposed to fetal bovine serum (FBS), resulting in distinct protein coronas on each nanoparticle. While PEGylation reduced brain cell internalization, PLGA nanoparticles were readily uptaken by microglia and neurons, with FBS-derived coronas further enhancing uptake. Pro-inflammatory immune responses were found to somewhat positively correlate with nanoparticle uptake levels, with any subsequent adverse effects on cell viability rescued by the presence of corona coatings. The formation of a protein corona is an inescapable phenomenon in biological fluids and has important implications for future NDDS and *in vitro* experimental design. The findings reported here highlight the role of the protein corona in mediating nanoparticle-cell interactions.

2. Results and discussion

Polymeric nanoparticles show promise as brain-targeted NDDS for neuronanomedicine. Their versatile synthesis allows control over composition, size, drug loading/release, and surface ligands for active delivery across the BBB into brain cells (e.g., BBB-penetrating moieties). Moreover, polymeric nanoparticles exhibit high biocompatibility, biodegradability, and, in most cases, low toxicity [12–14].

PLGA is an FDA-approved biodegradable polymer widely utilized in synthesizing nanoparticles to develop neuronanomedicine candidates [15, 16]. PLGA particles are frequently PEGylated to reduce protein corona formation, thereby helping to mitigate unwanted interactions in the body [17, 18]. Protein corona formation on both PLGA and PLGA-PEG particles has previously been studied both *in vitro* and *in vivo* [19, 20]. However, despite extensive research on the therapeutic applications of these polymeric particles, including clinical trials for brain-related disorders, such as neurodegenerative diseases [21], the effects of protein corona formation on the interaction between these particles and key brain cell subtypes remain understudied, with only 6 studies being reported in the literature to our knowledge [3, 7–11]. Accordingly, in this study, we opted to utilize both PLGA and PLGA-PEG nanoparticles as neuronanomedicine models to investigate the role of corona formation in mediating their cellular uptake activity in various brain cell subtypes.

As illustrated in schematic 1, PLGA and PLGA-PEG nanoparticles were synthesized and incubated with FBS to develop corona–nanoparticle complexes, which were characterized via proteomic analysis. These complexes were then interacted with several different brain cell subtypes (i.e. differentiated neurons; microglia; astrocytes), and the effect on cellular uptake, cell viability, and immune responses was evaluated.

2.1. Polymeric nanoparticles develop protein coronas upon exposure to FBS

We synthesized PLGA and PLGA-PEG polymeric nanoparticles using an emulsification-solvent evaporation technique [22], and then characterized their physical properties (figure 1). Dynamic light scattering (DLS) revealed that PLGA particles had a mean hydrodynamic diameter of 124 nm, with a polydispersity index (PDI) of 0.10, indicating homogeneity. Zeta potential analysis confirmed the PLGA

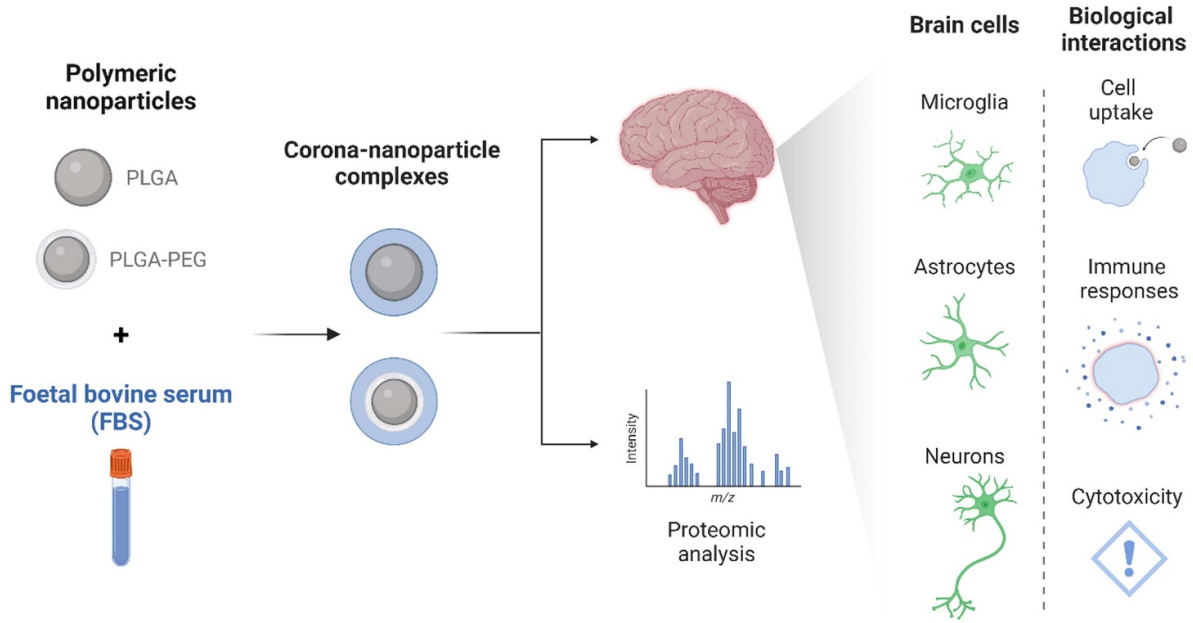

Schematic 1. Experimental workflow to investigate the development of FBS-derived coronas on polymeric nanoparticles and how they affect nanoparticle interactions with brain cells.

nanoparticles had negatively charged surfaces, with an overall net charge of −8 mV. On the other hand, PLGA-PEG nanoparticles were smaller at 77 nm with a PDI of 0.10, and had a more negative charge of −34 mV. Scanning electron microscopy (SEM) visualization confirmed the highly uniform and spherical shape of both nanoparticles (figures 1(a) and (f)). Both nanoparticles fall within the accepted size range for neuronanomedicines, as particles below 200 nm are known to cross the BBB and enter the brain [23].

Corona formation is influenced by a nanoparticle's physicochemical properties (e.g., size, shape, surface charge), as well as the biological fluid it interacts with and the duration of contact [24, 25]. With two physically distinct polymeric nanoparticles in hand, we set out to investigate the time-dependent formation of protein coronas on their surfaces after exposure to FBS. FBS was chosen as a model biological fluid as it has been used in >580 nanoparticle-protein corona studies [26], and due to its ease of availability. Following surface area adjustment, PLGA and PLGA-PEG nanoparticles were incubated with FBS at 37 °C, and any subsequent changes in particle size, charge, and protein adsorption were tracked for 12 h.

Over the 12 h incubation period, PLGA nanoparticles increased from 124 nm to a maximum size of 178 nm (figure 1(b)), representing a 1.4-fold size increase, while PLGA-PEG particles enlarged from 77 nm to 147 nm (figure 1(g)), showing a 1.9-fold increase. Despite significant size increases for both nanoparticles, the suspensions remained homogeneous and did not aggregate, with a consistently maintained PDI of 0.12. Concurrently, the zeta-potential for both particles became less negative over time, with PLGA nanoparticles shifting from −8 mV to −2 mV (figure 1(c)) and PLGA-PEG particles changing from −34 mV to −17 mV (figure 1(h)). These changes in biophysical properties were expected as the adsorption of serum proteins to the surface of nanoparticles has consistently been shown to increase their hydrodynamic radius and increase zeta potential to become less negative [27–30].

The total amount of FBS-derived protein absorbed onto the surface of both nanoparticles over time was quantified by Bradford assay. As expected, protein adsorption gradually increased to 980 μg ml^{-1} for PLGA nanoparticles and to 769 μg ml^{-1} for PLGA-PEG by 12 h incubation (figures 1(d) and (i)). Next, proteins bound to the nanoparticles' surfaces were desorbed and visualized by SDS-PAGE. This showed time-dependent increases in band intensity, reflecting the gradual adsorption of proteins onto the nanoparticles' surfaces, with distinct band patterns observed for each nanoparticle type (figures 1(e) and (j)).

The pronounced changes in biophysical characteristics observed after longer incubation times are particularly relevant to neuronanomedicine, where an effective NDDS must remain stable *in vivo* for extended periods [31].

Protein coronas undergo a 'hardening' process over time, in which highly abundant proteins bind first to the nanoparticle and are later exchanged by those with greater affinity (i.e. the Vroman effect) [32]. This transition leads to the formation of a stable and tightly bound 'hard corona' directly on the nanoparticle surface, accompanied by a 'soft corona,' which is a rapidly exchanging outer layer of molecules that is loosely bound to the hard corona [33]. We specifically focused on 'hard corona' formation; thus, corona-coated nanoparticles underwent thorough washing to remove unbound and loosely bound serum proteins before downstream analysis. Based on our findings above, we elected to next analyze the composition of the 'hard coronas' on the nanoparticles after 6 h and 12 h contact times with FBS, as this is a more stable, tightly bound corona.

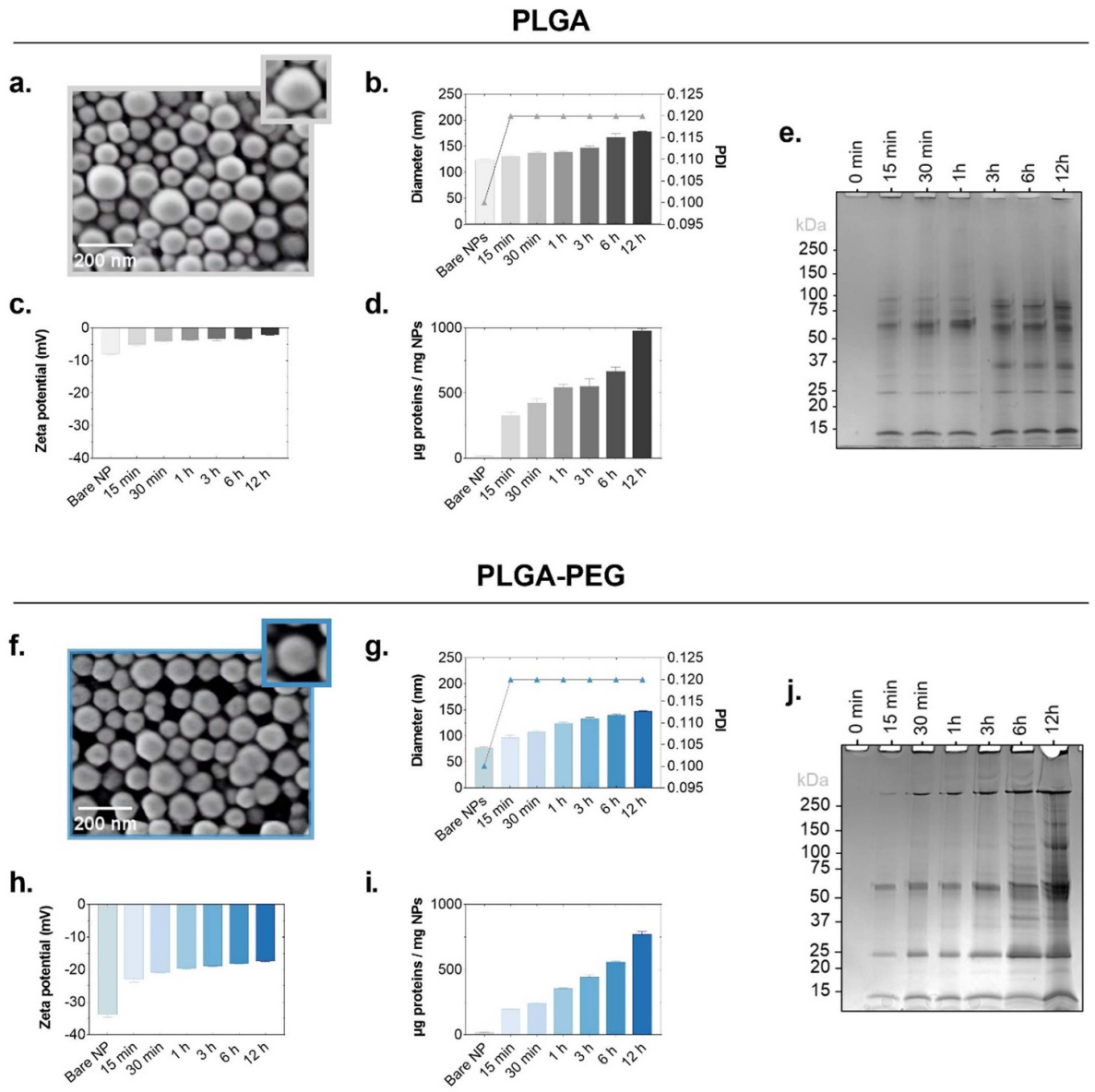

Figure 1. Development of FBS-derived protein coronas on the surfaces of polymeric nanoparticles. SEM images visualized spherical (a) PLGA and (f) PLGA-PEG nanoparticles. Scale bar = 200 nm. PLGA (upper panel; grey) and PLGA-PEG (lower panel; blue) particles were incubated with FBS for 15 min, 30 min, 1 h, 3 h, 6 h and 12 h, and their biophysical properties characterized. Over a 12 h period: (b), (g) DLS measurement revealed increasing size with no effect on monodispersity (PDI); concurrently, (c), (h) zeta potential analysis (mV) showed a shift toward less negative surface charge; (d), (i) total protein adsorption on nanoparticle surfaces increased steadily; (e), (j) SDS-PAGE analysis revealed protein band patterns that suggested compositional differences between nanoparticle–corona complexes. Results presented as mean ± SD.

2.2. The composition of FBS-derived protein coronas

The formation and composition of protein coronas are significantly determined by the physicochemical properties of a nanoparticle's surface, culminating in a distinctive biological fingerprint or barcode unique to the corona–nanoparticle complex [4, 24, 25]. To identify individual proteins within coronas and gain a detailed snapshot of corona composition, we digested proteins adsorbed on nanoparticle surfaces with trypsin and subjected them to liquid chromatography mass spectrometry (LC–MS) analysis. The identified proteins were subsequently categorized based on size, hydrophobicity, charge and function (figure 2 and supplementary figure S1).

In terms of contact time, a high degree of similarity was observed in the compositions of FBS coronas formed on each nanoparticle after 6 h and 12 h. Specifically, the top 20 most abundant proteins at each time-point were 90% and 85% identical on PLGA and PLGA-PEG particles, respectively (supplementary figure S1). Moreover, in the categories analyzed (i.e. size, hydrophobicity, charge, function), only a handful of small differences were determined between 6 h and 12 h coronas on PLGA nanoparticles, whereas none were

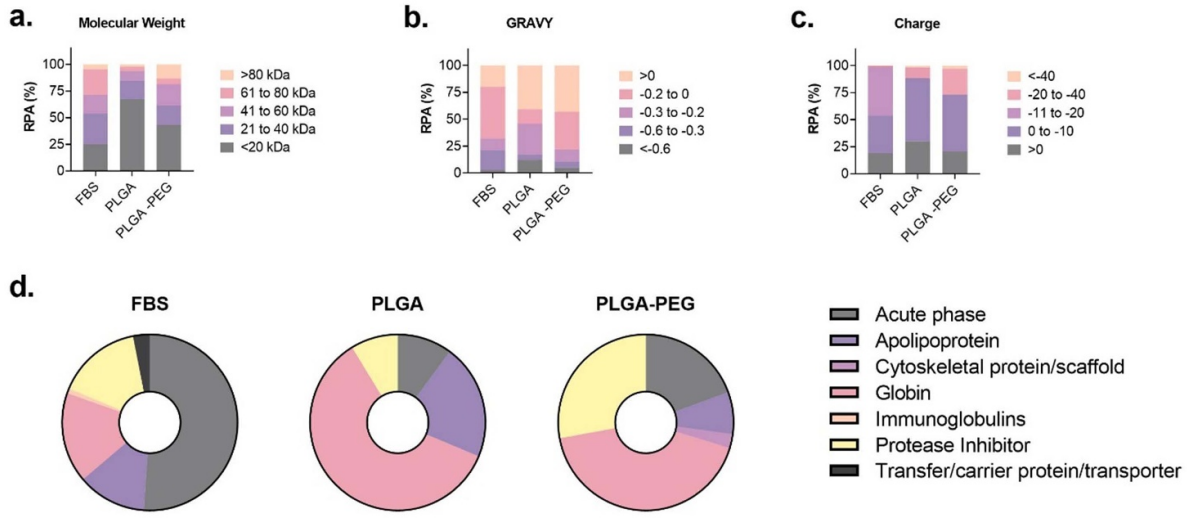

Figure 2. LC–MS analysis of FBS-derived protein coronas on polymeric nanoparticles. After incubating nanoparticles with FBS for 6 h, adsorbed proteins were detached from particle surfaces, analyzed by LC–MS, and then bioinformatically evaluated to determine their: (a) molecular weight; (b) hydropathicity; (c) charge at pH 7.4; and (d) functional classification. Results are presented as the relative protein abundance (%) of the top 20 proteins in each corona, or the FBS source fluid.

present for coronas on PLGA-PEG particles. Due to the similarity at both time-points, the 6 h corona–nanoparticle complexes were chosen for further in-depth investigation (compositional analysis of 12 h corona–nanoparticle complexes are provided in supplementary figure S2). The similarity observed between the 6 and 12 h coronas is somewhat expected, as the initial corona formation involves rapid protein association/dissociation, eventually reaching an equilibrium approximately 3–24 h later [30, 34].

Both polymeric nanoparticles showed a preference for adsorbing low molecular weight (MW) proteins (<20 kDa), consistent with previous findings in the corona literature (figure 2(a)) [35]. The PLGA corona was composed of 67% low-MW FBS proteins, an almost 3-fold higher concentration than FBS itself. Conversely, high-MW proteins (>61 kDa) accounted for only 6% of the PLGA corona. In contrast, the PLGA-PEG corona had a lower proportion of low-MW proteins (44%) compared to its PLGA counterpart but contained a higher percentage of high-MW proteins (18%).

When compared to FBS, grand average of hydropathicity (GRAVY) scores indicated that both coronas accumulated hydrophobic proteins (GRAVY >0; figure 2(b)). While 20% of FBS was composed of hydrophobic proteins, they accounted for 41% and 43% of coronas on the PLGA and PLGA-PEG particles, respectively, a more than 2-fold increase. At physiological pH 7.4, coronas had a high abundance of proteins that were less negatively charged (figure 2(c)). Proteins with net charges between 0 to −10 mV or >0 mV constituted 54% of FBS, but 88% of the PLGA corona and 77% of its PLGA-PEG counterpart.

Finally, the LC/MS identified proteins were categorized into functional classes using the PANTHER classification system (figure 2(d)) [36]. FBS source fluid exhibited a predominance of acute phase proteins (51%) and, to a lesser extent, globins (17%). In contrast, protein coronas on PLGA nanoparticles showed elevated levels of globins (60%) and apolipoproteins (21%). The composition of PLGA-PEG nanoparticle coronas differed notably, with lower levels of globins (42%) but distinctly higher amounts of protease inhibitors (28%).

2.3. Specific proteins show enrichment/depletion in corona–nanoparticle complexes

Protein corona formation is a dynamic, competitive, and time-dependent process [24, 32]. Based on our observation of distinct protein coronas formed on the two polymeric nanoparticles, we conducted a more detailed analysis of their composition. This involved identifying and scrutinizing the top 20 proteins in each corona (table 1 and supplementary table S1), followed by an assessment of their enrichment/depletion in relation to the FBS source fluid (figure 3 and supplementary figure S2).

In FBS, acute phase proteins were predominant, with the two most abundant proteins being α-2-HS-glycoprotein (fetuin; 30%) and albumin (13%). These proteins were depleted in the coronas on both polymeric nanoparticles (figure 3), reducing to 5% and 4% in the PLGA corona, and 13% and 4% in the PLGA-PEG corona, respectively (table 1). The depletion of albumin, a highly abundant but low-affinity protein in FBS, can be attributed to its displacement by lower abundance yet higher affinity proteins such as apolipoproteins [27, 37]. Indeed, this recognized phenomenon is evident in the PLGA nanoparticle corona, where the abundance of apolipoproteins (21%) is highly enriched compared to FBS (13%). Moreover, the most abundant apolipoprotein in the PLGA corona was apolipoprotein A-I (ApoAI; 10%), the second most abundant apolipoprotein in the cerebral spinal fluid, the fluid surrounding the brain. ApoAI plays a key role in energy metabolism and may play a role in Alzheimer's disease and

Table 1. The top 20 most abundant proteins present in the protein coronas adsorbed onto PLGA and PLGA-PEG nanoparticles, and their relative abundance (RPA %). Proteins are listed in alphabetical order.

		PLGA		PLGA-PEG	
Accession	**Protein description**	**Rank**	**% RPA**	**Rank**	**% RPA**
P60712|ACTB_BOVIN	Actin, cytoplasmic 1			16	1.3%
P63258|ACTG_BOVIN	Actin, cytoplasmic 2			17	1.3%
P02769|ALBU_BOVIN	Albumin	9	3.7%	8	3.9%
P34955|A1AT_BOVIN	Alpha-1-antiproteinase	4	6.3%	3	12.6%
P12763|FETUA_BOVIN	Alpha-2-HS-glycoprotein (Fetuin)	6	5.4%	2	13.2%
Q7SIH1|A2MG_BOVIN	Alpha-2-macroglobulin			19	1.2%
P01017|ANGT_BOVIN	Angiotensinogen	10	1.8%	9	3.8%
P15497|APOA1_BOVIN	Apolipoprotein A-I	3	10.4%	6	4.8%
P81644|APOA2_BOVIN	Apolipoprotein A-II	8	4.0%		
Q32PJ2|APOA4_BOVIN	Apolipoprotein A-IV	18	0.9%		
E1BNR0|E1BNR0_BOVIN	Apolipoprotein B	11	1.7%	11	2.9%
P19034|APOC2_BOVIN	Apolipoprotein C-II	14	1.3%		
P19035|APOC3_BOVIN	Apolipoprotein C-III	16	1.1%		
Q03247|APOE_BOVIN	Apolipoprotein E	15	1.2%		
F1MYX2|F1MYX2_BOVIN	Apolipoprotein M	19	0.7%		
Q2UVX4|CO3_BOVIN	Complement C3			13	1.7%
A0A452DIQ5|A0A452DIQ5_BOVIN	GLOBIN domain-containing protein	2	21.8%		
G3N1Y3|G3N1Y3_BOVIN	GLOBIN domain-containing protein	7	5.4%	5	9.7%
P02081|HBBF_BOVIN	Hemoglobin fetal subunit beta	5	5.7%	4	10.0%
P01966|HBA_BOVIN	Hemoglobin subunit alpha	1	24.1%	1	18.6%
P02070|HBB_BOVIN	Hemoglobin subunit beta	13	1.4%	7	4.1%
F1MMI1|F1MMI1_BOVIN	Hemoglobin subunit zeta	12	1.6%		
A0A3Q1LK49|A0A3Q1LK49_BOVIN	Inter-alpha-trypsin inhibitor heavy chain H2	20	0.6%	12	2.2%
P56652|ITIH3_BOVIN	Inter-alpha-trypsin inhibitor heavy chain H3			14	1.3%
Q3T052|ITIH4_BOVIN	Inter-alpha-trypsin inhibitor heavy chain H4			10	3.7%
Q95121|PEDF_BOVIN	Pigment epithelium-derived factor			18	1.2%
F6R4P6|F6R4P6_BOVIN	Serpin family D member 1			15	1.3%
O46375|TTHY_BOVIN	Transthyretin	17	1.0%	20	1.2%

schizophrenia [38]. Therefore, there may be potential functional consequences for brain cells related to up-regulation of these proteins within the FBS-derived PLGA corona.

The most enriched functional protein group in PLGA and PLGA-PEG coronas was globins, with hemoglobins accounting for approximately 60% of PLGA coronas and 42% of PLGA-PEG coronas, over twice that of FBS (17%). Previous investigations into protein-nanoparticle interactions have demonstrated that hemoglobin exhibits higher binding affinities to the surfaces of near-neutral (−4 mV) and negative (−13 mV) polymer-coated nanoparticles than both albumin and fetuin [39, 40]. This suggests that, in our study, hemoglobin may indeed play a role in replacing both albumin and fetuin on the surface of both PLGA (−3 mV) and PLGA-PEG (−18 mV) nanoparticles due to its greater binding affinity. However, this may have consequential effects on long-term safety for potential FBS-PLGA NDDSs. Circulating hemoglobin and its degradation products can be neurotoxic, and hemoglobin levels have been shown to be upregulated in several neurodegenerative diseases [41, 42]. Therefore, elevated extracellular neurological hemoglobin due to an NDDS in an already vulnerable environment, such as in neurological disorders may outweigh or counteract benefits due to delivered therapeutics within the NDDS.

The PLGA-PEG protein corona was also enriched in protease inhibitors (28%), with the third most abundant protein being alpha-1-antiproteinase (A1AT; 13%; behind hemoglobin subunit-alpha and fetuin). This protein is presumed to have high binding affinity, as it is consistently detected in coronas derived from FBS, irrespective of the nanoparticle formulation [35, 43].

Despite some similarities with previous reports of FBS-derived protein coronas on PLGA and PLGA-PEG nanoparticles [27, 35], there are notable differences in our findings. For instance, complement proteins (e.g., Complement C3, C4) are not among the top 20 identified proteins in the PLGA corona [27], and proteins categorized as 'protease inhibitors' are more frequently detected compared to other studies on PLGA-PEG corona formation [35]. These differences in protein enrichment/depletion may be attributed to the longer incubation times used in our study, which resulted in the detection of >800 proteins in corona–nanoparticle complexes, whereas some others have reported fewer than 40 proteins in the PLGA and PLGA-PEG coronas following a 30 min incubation [27, 35]. In line with this, our study demonstrated a gradual increase in corona size and protein adsorbence over time, suggesting that 30 min incubation may not be sufficient to see full formation of the protein corona.

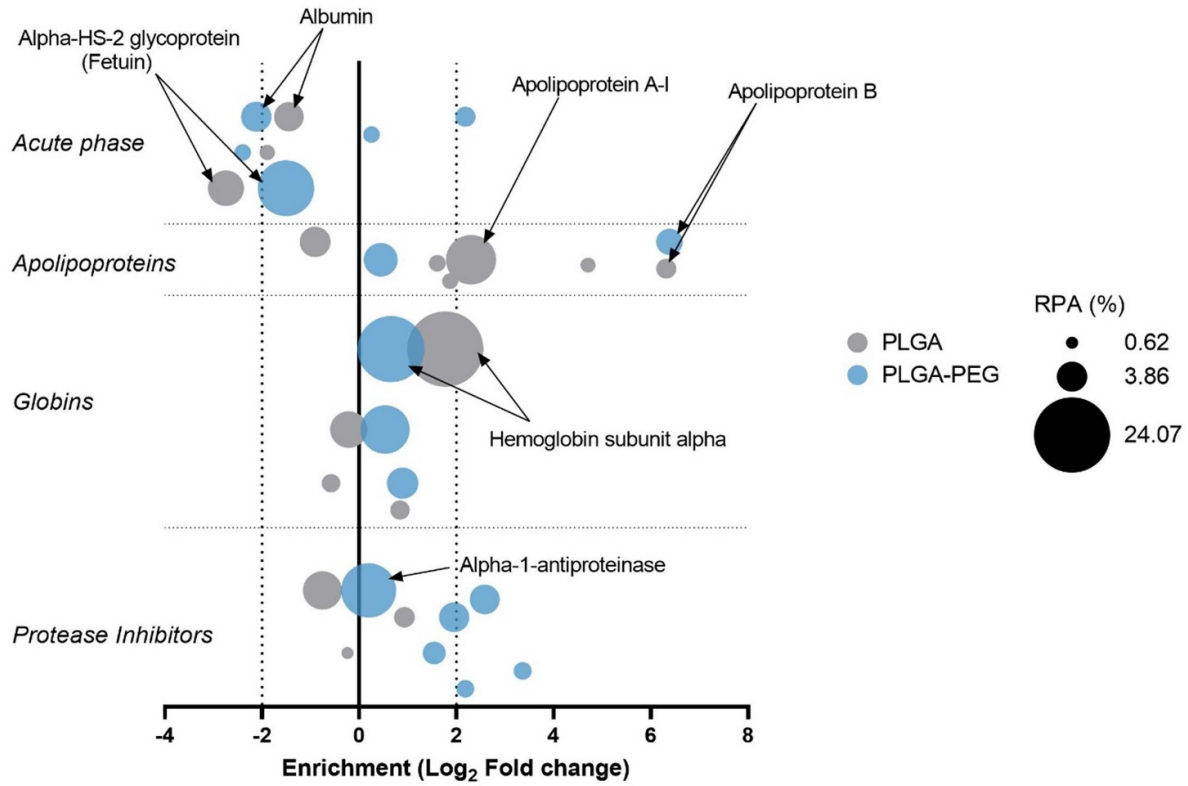

Figure 3. Compositional map depicting the protein enrichment/depletion in corona–nanoparticle complexes. Proteins were compared (i.e. Log_2 fold-change) to the FBS source fluid to establish enrichment (>0) or depletion (<0) of proteins within coronas. Proteins are grouped by functional class; and circle size corresponds to the relative protein abundance (RPA %) within the top 20 proteins determined by LC/MS. Proteins of interest are annotated.

2.4. FBS coronas augment the uptake of polymeric nanoparticles by brain cells

Protein coronas modulate nanoparticle-cell interactions, capable of either enhancing or hindering cellular uptake [44]. Some corona proteins act as ligands, directing particles to specific cell receptors and promoting internalization, while others can influence cell recognition and uptake (e.g., dysopsonins prevent particle phagocytosis by immune cells) [36]. Moreover, dense corona coatings are known to mask targeting ligands on nanoparticles (e.g., cell-specific antibodies), stopping them from mediating targeted delivery [8].

The brain is composed of specialized cell types, each with a unique gene expression pattern, that are essential for its proper function, including, among others, neurons for signal transmission, microglia for immune defense and brain maintenance, astrocytes for structural support and metabolic assistance to neurons, and endothelial cells that form the protective BBB [45, 46]. To recapitulate brain structure and function for testing neuronanomedicines *in vitro*, researchers typically rely upon immortalized cell lines to streamline experiments and minimize cost, while also reducing concerns around yield, maturity of cells obtained and ethical issues inherent to work with primary cells or induced pluripotent stem cells [47–49]. Consistent with the above strategy, we proceeded to investigate the effect protein corona composition has on the internalization of PLGA and PLGA-PEG nanoparticles by cells representing the brain parenchyma: BV-2 murine microglial cells; 1321N1 human astrocytoma cells; and SH-SY5Y human neuroblastoma cells differentiated into neurons. As we were interested in the discrete effects on each cell type in the first instance, we elected to investigate each in isolation, rather than using a co-culture model.

Each brain cell subtype was co-incubated with fluorescent Fluorescein isothiocyanate isomer 1 (FITC)-loaded nanoparticles, with and without protein corona coatings, in serum-deprived media for 6 h. Next, nanoparticle uptake by each brain cell subtype was quantified using flow cytometric analysis, with representative images obtained via confocal fluorescent microscopy (figure 4).

As depicted in figure 4(a), 45% of microglial cells internalized bare PLGA particles, which increased significantly to 55% with FBS-derived coronas ($p = 0.0124$). This finding is unsurprising, as microglia naturally recognize and phagocytose nanoparticles, with corona coatings also known to further enhance phagocytosis [50]. The observed increase in uptake of corona-coated PLGA particles might be partly due to the elevated hemoglobin content in the corona, as hemoglobin readily interacts with microglial cells via receptor- and phosphatidylserine-mediated phagocytotic mechanisms [51, 52]. Similarly, the adsorption of hemoglobin onto near-neutral nanoparticles, like the PLGA particle herein, can

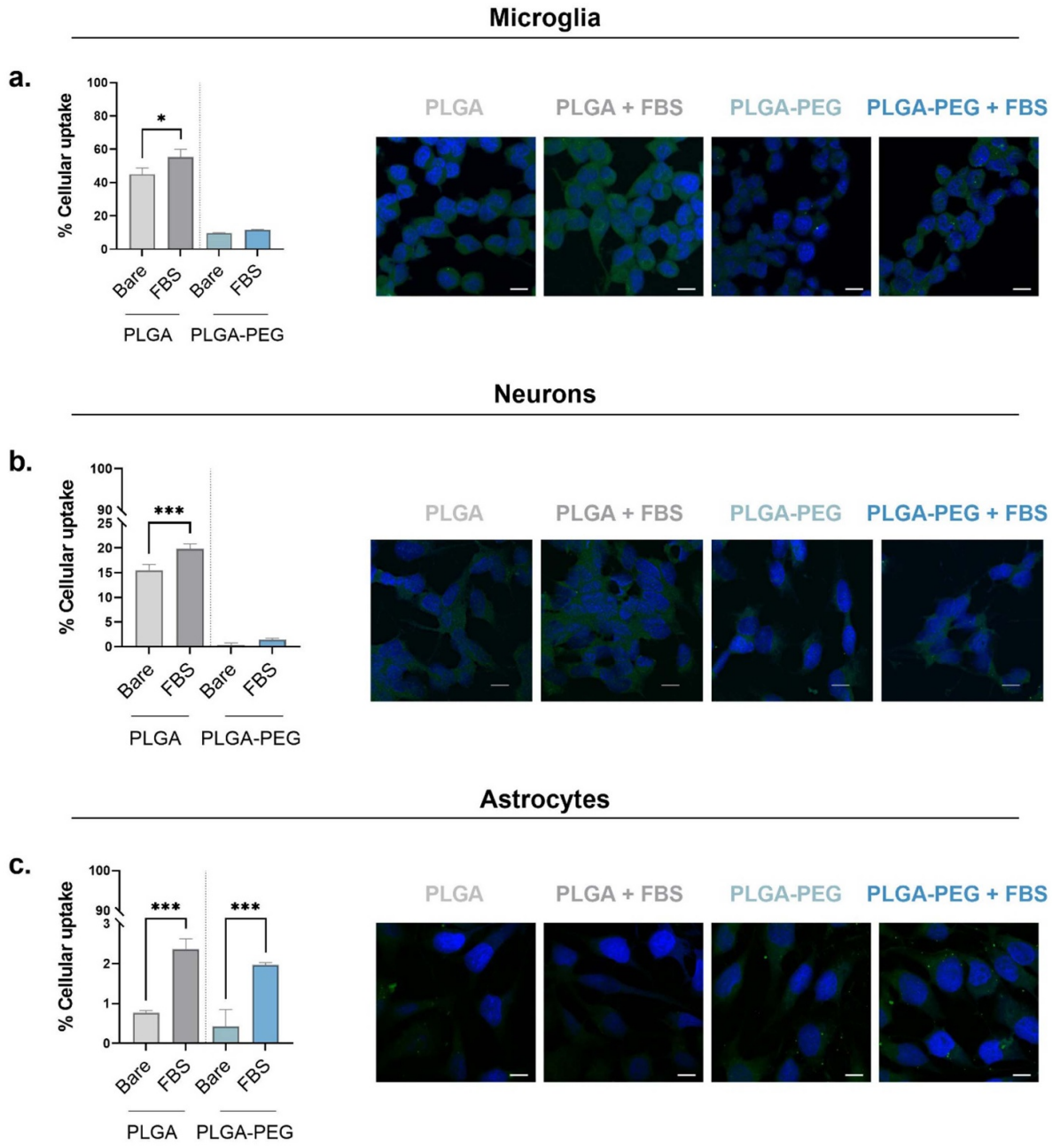

Figure 4. Uptake of corona–nanoparticle complexes by various brain cell subtypes. Fluorescent FITC-loaded PLGA or PLGA-PEG particles were coated with FBS coronas and incubated for 24 h with (a) microglia; (b) neurons; (c) astrocytes. (Left) Fluorescent histograms from flow cytometry depict the cellular uptake (%) of corona–nanoparticle complexes. Error bars represent mean ± SD. Statistical significance determined via two-way ANOVA, with Šídák post-hoc analysis ($^{*}p \leqslant 0.05$, $^{***}p \leqslant 0.001$), $n \geqslant 3$, from three independent experiments. (Right) Representative fluorescence microscopy images (merged) show the cellular internalization of corona–nanoparticle complexes (green); DAPI-stained cell nuclei (blue); scale bars = 10 μm.

induce changes in its secondary structure and lead to enhanced immune cell recognition [39]. Further, as discussed above, given the neurotoxicity of extracellular hemoglobin, it is unsurprising that microglia could be primed to recognize and phagocytose these particles. Conversely, ApoAI constitutes 10% of the PLGA corona and is a recognized dysopsonin that enables nanoparticles to evade the immune system. However, considering that the abundance of ApoAI in the PLGA corona is three times lower than hemoglobin, its dysopsonizing effects are likely attenuated in this case.

On the other hand, minimal cellular uptake by microglia was observed for bare (10%) and FBS-coated (12%) PLGA-PEG nanoparticles. Interestingly, despite the PLGA-PEG corona comprising ∼30% hemoglobin, there was no significant difference in uptake when compared to uncoated particles ($p = 0.8593$). This could be due to two reasons:

the 'stealth' effect conferred by PEGylation which minimizes the corona size/density; and the dysopsonizing nature of fetuin which makes up 13% of the PLGA-PEG corona [39]. Additionally, A1AT, which comprised 13% of the PLGA-PEG corona, has been shown to have potent anti-inflammatory and anti-apoptotic activities [53, 54]. The presence of A1AT, in combination with fetuin, in the PLGA-PEG protein corona may have resulted in decreased microglial activation, with A1AT shown to induce microglial polarization towards an M2 phenotype [54], making them less likely to internalize these particles.

Figure 4(b) shows that 16% of neuronal cells internalized bare PLGA nanoparticles, which significantly increased to 20% with presence of an FBS corona ($P = 0.0008$). Conversely, the uptake of PLGA-PEG particles, without or with coronas, was minimal (<2%). This relatively high uptake even by bare particles is in line with previous literature showing that neurons differentiated from SH-SY5Y cells are capable of taking up silica nanoparticles, without altering neurite outgrowth, but with reductions in neural differentiation [55]. Additionally, the high uptake of bare PLGA particles may result from protein corona formation during incubation with neurons. Unlike microglia and astrocytes, SH-SY5Y-derived neurons require serum for survival, so nanoparticle uptake experiments with these cells were conducted in media supplemented with 1% FBS [56]. This set-up may have led to a small degree of FBS corona formation on the bare nanoparticles, potentially enhancing their uptake. Despite this, the overall internalization of corona-coated PLGA nanoparticles was still 25% higher than that of the bare particles. This may be due to the presence of apolipoproteins in the corona. Apolipoproteins are known to be high affinity-low abundance proteins [37], and thus may not have had sufficient time to bind to bare particles in FBS supplemented culture media. Apolipoproteins, specifically apolipoprotein E, which constituted 1.2% of the PLGA corona, are known to facilitate nanoparticle uptake into neurons by binding low density lipoprotein receptors [57].

With astrocytes (figure 4(c)), we observed statistically significantly higher uptake of corona-bearing PLGA ($p = 0.0002$) and PLGA-PEG ($p = 0.0003$) nanoparticles over bare particles; however, the observed internalization remained below 3%, suggesting negligible uptake. This almost complete absence of uptake is surprising, especially given that, in some reported cases, nanoparticles are more readily internalized by astrocytes than neurons [58, 59]. For example, Haase and colleagues (2012) indicated greater uptake of and subsequent vulnerability (as evidenced by morphological changes) to silver nanoparticles in astrocytes as compared to neurons [59]. Moreover, 1321N1 human astrocytoma cells used in this study have been previously shown to endocytose other polymeric nanoparticle types via classical clathrin-mediated mechanisms [60]. It is important to note, however, that the 1321N1 astrocytes used in the current study were at baseline state and were not pre-stimulated, for example with lipopolysaccharide (LPS), which may have better modelled the pro-inflammatory brain environment seen in many neurological disorders and enhanced nanoparticle uptake [58].

Our study determined that PLGA nanoparticles coated with FBS-derived coronas exhibited the highest uptake across immune and non-immune neuro-derived cells (Microglia > Neurons > Astrocytes). Meanwhile, the low or near-complete absence of PLGA-PEG particle uptake corresponds with PEG's 'stealth' characteristics, consistent with previous reports suggesting that PEGylated nanoparticles can reduce internalization by brain cell subtypes [10]. The surprising lack of uptake of polymeric nanoparticles by astrocytes (with and without coronas) highlights the variability in internalization mechanisms among different cell types and the potential importance of cellular environment in influencing uptake [60]. Also, considering that PLGA particles with different surface chemistries have previously shown varying cell uptake pathways in microglia [50], further investigations into the underlying brain cell-uptake mechanisms associated with the nanoparticle–corona complexes from this study are warranted.

Collectively, these findings suggest that nanoparticle-corona properties could be 'tuned' to selectively deliver NDDS to neurons over astrocytes, potentially allowing corona-mediated targeting of neuron-specific pathologies (e.g. Lewy bodies in Parkinson's disease; neurofibrillary tangles in Alzheimer's disease). In one example of this strategy, Zhang *et al* modified the surfaces of liposomal nanoparticles with non-toxic amyloid-beta derived peptides [9]. Upon systemic administration into mice, this surface modification enabled the selective adsorption of serum apolipoproteins, which then facilitated the receptor-mediated transcytosis of the nanoparticles across the BBB [9].

2.5. FBS coronas influence brain cell responses to polymeric nanoparticles

Polymeric nanoparticles show preclinical promise in treating brain disorders, but questions remain about their potential neurotoxicology, particularly in regard to their degradation processes and byproducts [61, 62]. We therefore sought to investigate the influence protein coronas have on cellular and immune responses to both PLGA and PLGA-PEG nanoparticles

While performing uptake experiments (figure 4), we collected supernatants from cells exposed to corona–nanoparticle complexes and measured the secretion of pro-inflammatory cytokines, tumor necrosis factor (TNF) and interleukin (IL)-6 (figure 5). Both cytokines are associated with neuroinflammation and neurotoxicity; TNF contributes to the initiation and amplification of inflammation, while IL-6 regulates immune responses and metabolic processes [63, 64].

In close correlation with cellular uptake data (figure 4), microglial cells treated with corona-bearing PLGA nanoparticles secreted the greatest amount of TNF (673 pg ml^{-1}; figure 5(a)), while bare particles induced 83% less TNF secretion (111 pg ml^{-1}). In contrast, PLGA-PEG nanoparticles (without or with coronas) induced ∼50-fold less cytokine release (<13 pg ml^{-1}; figure 5(b)), which again correlates with their much lower uptake. The high TNF production

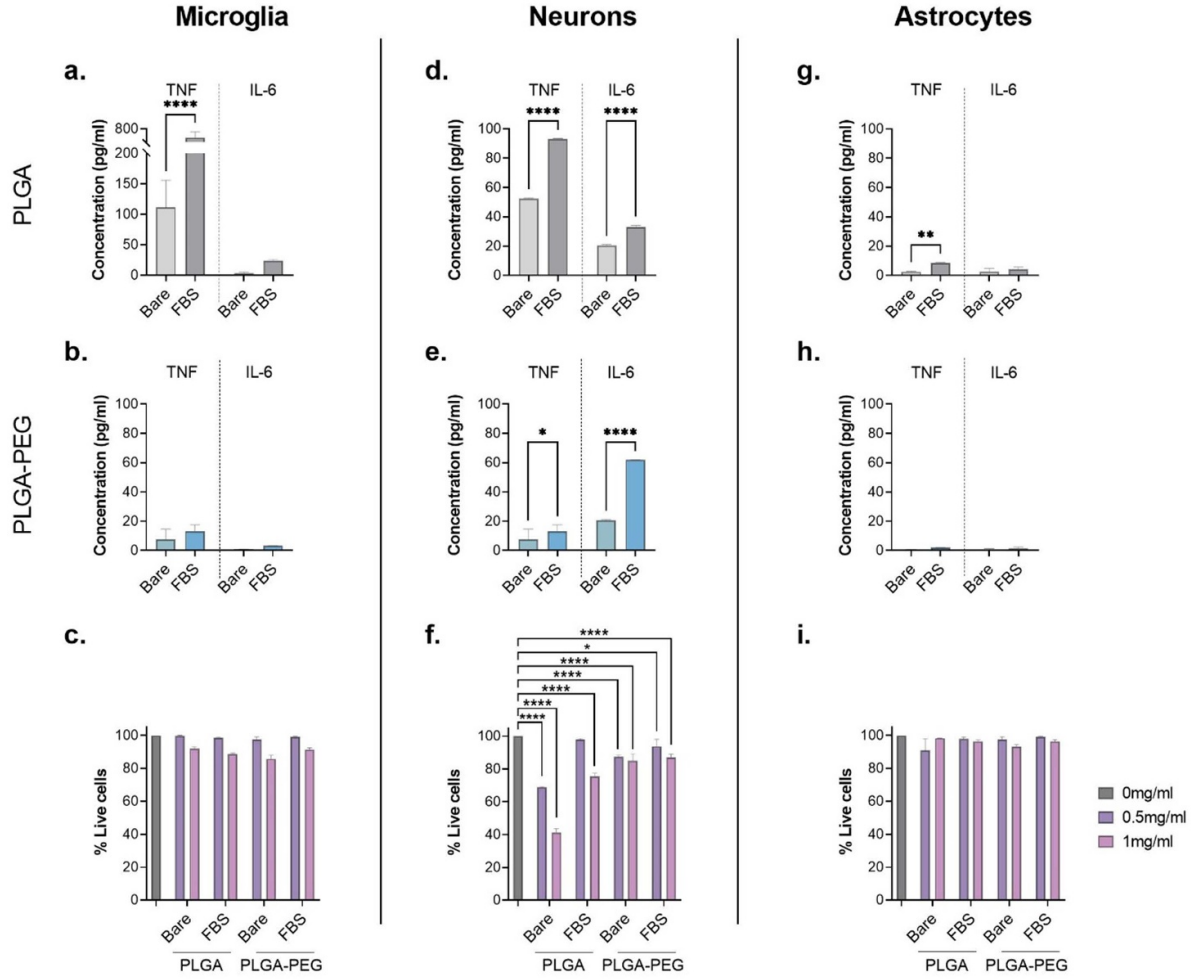

Figure 5. Inflammatory responses of brain cell types to corona–nanoparticle complexes and effect on brain cell viability. Polymeric nanoparticles (with and without FBS coronas) were incubated for 6 h with microglia (left panel), neurons (middle panel), and astrocytes (right panel). After treatment with (a), (d), (g) PLGA or (b), (e), (h) PLGA-PEG particles the concentration (pg ml^{-1}) of pro-inflammatory cytokines TNF-α and IL-6 secreted by cells was quantified by cytokine bead array. (c), (f), (i) Viability of brain cells after exposure to different concentrations of polymeric nanoparticles (with and without coronas) was determined by MTT assay. Results presented as mean $\pm$ SD. Statistical significance determined via two-way ANOVA, Tukey's (a), (b), (d), (e), (g), (h) or Dunnett's (c), (f), (i) post-hoc analysis ($^{*}p \leqslant 0.05$, $^{****}p \leqslant 0.0001$).

induced by the corona-coated PLGA particles in particular raises some potential concerns, given that normal TNF levels in human serum are 0–4 pg ml^{-1} [65]. Within the brain, excessive microglial activation and overproduction of TNF induces neuroinflammation and can cause collateral neuronal damage, a process observed in neurodegenerative diseases [66, 67]. Nevertheless, microglia cells maintained over 80% viability even when exposed to nanoparticle concentrations up to 1 mg ml^{-1}(figure 5(c)), suggesting negligible microglial toxicity, although further investigations, particularly in *in vivo* models of neurological disease where longer follow-up timepoints are possible, are warranted. Of note, while increases in microglial IL-6 release were not noted in the current work, this may be because of the 6 h follow-up timepoint. In line with this, IL-6 release from microglia in culture was not detectable until 4–6 h, even following stimulation with LPS, as opposed to TNF, which was detectable in the supernatant within 1–2 h [68]. This suggests that, to see alterations in IL-6 release from microglia, longer follow-up timepoints may be required.

Neurons similarly showed high levels of TNF release after incubation with bare PLGA nanoparticles (52 pg ml^{-1}), which significantly increased by 77% with the presence of an FBS corona (93 pg ml^{-1}) (figure 5(d)). Low levels of TNF secretion were also detected from neurons treated with PLGA-PEG nanoparticles without (8 pg ml^{-1}) or with (13 pg ml^{-1}) coronas. Interestingly, neurons were the only brain cell subtype to secrete substantial amounts of IL-6 at 6 h when exposed to polymeric nanoparticles (with and without coronas). Specifically, we observed that FBS coronas increased IL-6 release, while corona-coated PLGA-PEG particles induced the highest IL-6 secretion overall (figure 5(e)). Interestingly, TNF has been shown to induce IL-6 release in cultures of murine cortical neurons [69]. The timeline of IL-6 release from neurons may also be different than that noted for microglia. In line with this, studies in humans following traumatic spinal

cord injury have demonstrated increased immunoreactivity of IL-6 within neurons, but not microglia, as early as 30 min following injury. Conversely, IL-6 immunoreactivity was elevated in both neurons and microglia by 5 h post-injury [70]. This may, at least in part, help to explain why increases in IL-6 release from neurons, but not microglia, were noted at 6 h follow-up in the current study, although further work to understand the mechanisms of action via which the protein corona can exacerbate this release is needed.

As depicted in figure 5(f), neuronal cell viability decreased to as low as 41% when treated with bare PLGA nanoparticles (1 mg ml^{-1}) but was subsequently rescued when particles were coated with an FBS corona. It is also worth noting that *in vitro* neuroinflammation and neurotoxicity do not necessarily translate *in vivo*. For example, brain-penetrating polymeric polybutylcyanoacrylate nanoparticles were previously found to cause brain cell death at high doses *in vitro*, yet rats treated with identical doses showed no signs of neuronal death [71].

Astrocytes showed no significant production of pro-inflammatory cytokines (figures 5(g) and (h)) and no reduction in cell viability (figure 5(i)) following exposure to polymeric nanoparticles, regardless of corona coatings. This is in line with other reports, in which PLGA and PLGA-PEG nanoparticles have been shown to be non-toxic to both primary and immortalized astrocyte cell lines [72, 73], and is also in line with our data showing extremely low uptake of the nanoparticles by these cells.

The results above suggest that FBS coronae influence cellular responses to polymeric nanoparticles. In particular, corona coatings induced increased cytokine secretion by microglia and neurons, but also mitigated cytotoxicity when nanoparticles came into contact with neurons. Such insights into the role protein coronas play in the neuroinflammatory and neurotoxic effects of nanoparticles can help inform downstream preclinical work and may have an important impact on the translation of NDDS to the clinic.

3. Conclusion

Our study highlights that the composition of protein coronas is largely determined by the physicochemical properties of the nanoparticles they form around. Furthermore, we discovered that corona composition significantly influences nanoparticle-brain cell interactions, affecting uptake efficiency, immune responses, and cytotoxicity.

The vast majority of corona–nanoparticle studies employ plasma and serum as the biological fluid source, with a recent systematic review revealing >80% of protein corona studies use these blood components [26]. Using FBS as a fluid source, a fluid used in over 32% of corona studies [26], we identified a high abundance of hemoglobins in protein coronas on polymeric nanoparticles, consistent with prior research [27, 35]. The presence of hemoglobin correlated with proinflammatory responses from some brain cells, aligning with the neurotoxicity of extracellular hemoglobin [42]. Considering this, and that brain cells are not exposed to serum proteins under healthy physiological conditions, FBS is likely not the optimal biological fluid for the *in vitro* study of protein coronas in neuronanomedicine. Indeed, recent work by Cox *et al* [74] described significant compositional changes in protein coronas during nanoparticle migration through an *in vitro* transwell BBB model. This suggests that coronas developed on systemically administered neuronanomedicines will change as they move from the bloodstream, across the BBB, into the brain parenchyma. Hence, further research into corona formation in cerebrospinal fluid (CSF), which can be challenging to obtain, is necessary, as it is better represents the brain microenvironment than serum.

In vitro models are essential for NDDS development, offering advantages such as cost-effectiveness, speed, simplicity, scalability and reduced ethical concerns compared to animal models. However, relying solely on them to predict NDDS performance *in vivo* is problematic. We investigated the biological effects of FBS-derived coronas on the interactions between nanoparticles and various immortalized human- and murine-derived brain cells in a 2D cell culture format. While these cell lines are commonly employed in neuroscience experiments, we acknowledge that expecting neutral (or similar) responses from human and murine cell lines to the bovine proteins in FBS may be unrealistic, and different results might be obtained under other conditions. Lastly, neurodegeneration is inherently an inflammatory disease [68], and, while outside the scope of this research, pre-stimulation of all the cell lines with inflammatory stimulants to more closely simulate disease conditions may reveal further differences in the behavior of the nanoparticles when interacted with cells.

Overall, for more precise *in vitro* evaluation of neuronanomedicine candidates, greater emphasis should be placed on selecting, and ensuring the compatibility, of biological fluids (i.e., type, origin, concentration) and brain cells. For example, exposing nanoparticles to human CSF and assessing the impact of the resulting corona–nanoparticle complexes on human-derived brain cells would yield more physiologically relevant experimental data. Additionally, physiological conditions are 3-dimensional, where brain cell types can have important interactions with one another. Therefore, co-culture models to evaluate the effect of these interactions and simultaneous/subsequent nanoparticle-protein corona-cell interactions should be incorporated into future work. Adopting such an approach in the future will benefit the advancement of neuronanomedicines and, ultimately, their translational outcomes.

4. Experimental section

4.1. Materials

Acid terminated PLGA copolymer (Resomer RG 503′ lactide:glycolide 50:50; Mw 24 000–38 000 Da); and poly(vinyl alcohol) (PVA; Mowiol 8–88; Mw ∼67 000 Da) were both procured from Sigma-Aldrich. PLGA-PEG-NH_2 copolymer (Mw 12 000–2000 Da) was sourced from Akina Inc (USA). FBS was acquired from ThermoFisher Scientific. All remaining chemicals and reagents utilized in this investigation were obtained from Sigma-Aldrich or ThermoFisher Scientific, unless otherwise specified.

4.2. Nanoparticle preparation and biophysical characterization

Nanoparticle synthesis: Polymeric nanoparticles were synthesized using the emulsification-solvent evaporation technique [22]. Briefly, PLGA or PLGA-PEG copolymer (30 mg) was dissolved in dichloromethane (DCM) (3 mL) and added dropwise to PVA (12.5 mL; 5%). For uptake studies, DCM was additionally supplemented with the green fluorescent dye (1 mg), FITC. The mixture was then sonicated using a microtip-probe sonicator (3 x 30 sec cycle, 100% amplitude), and shaken overnight to facilitate evaporation. Nanoparticles were collected by centrifugation (17 500 x*g*, 15 min), washed thrice to remove excess solvents, and finally resuspended in in ultrapure water and stored at 4 °C. FITC-loaded nanoparticles underwent further purification, whereby surplus dye was removed by overnight dialysis in PBS at 4 °C, utilizing Slide-A-Lyzer Dialysis Cassettes with a 10 kDa molecular cut-off, before being resuspended in water.

FITC-loaded nanoparticle dye entrapment efficiency: the amount of FITC encapsulated in the nanoparticles was determined by comparison to a standard curve of FITC. The entrapment efficiency (%) was then calculated using:

$$\text{Entrapment efficiency } (\%) = \frac{\text{Amount of FITC in nanoparticle}}{\text{Initial amount of FITC}} \times 100 \text{ [75].}$$

DLS: physical characteristics of nanoparticles, both bare and corona coated, were determined using a Zetasizer Nano ZS (Malvern instruments, UK) at 25 °C in ultrapure water. Diluted nanoparticles (0.15 mg ml^{-1}) were measured in technical triplicate to determine the hydrodynamic diameter (d.nm), PDI, and zeta potential (mV).

SEM: 0.1 mg of polymeric nanoparticles were dissolved in 1 ml acetone, with 10 μl of the resulting solution then placed onto a silicon wafer and left to dry overnight. Samples then underwent sputter-coating with gold-palladium using an EM ACE600 Sputter Coater (Leica, Germany). Lastly, SEM images of the nanoparticles were acquired on a SUPRA 55VP Field Emission-SEM at 5 kV and 65 000x magnification (ZEISS, Germany).

4.3. Protein corona formation and analysis

FBS adsorption onto polymeric nanoparticles was performed as per the method described by Partikel *et al* [25, 26] PLGA and PLGA-PEG particles were suspended in FBS such that the exposed surface area of each particle was equivalent ($A = 4\pi r^2$; $A = 0.08$ m^2). Nanoparticle suspensions were incubated for increasing amounts of time (15 min–12 h) with gentle agitation at 37 °C. Next, samples were purified to remove unbound/loosely bound proteins by >3 wash cycles in ultrapure water and then collected by centrifugation (21 000x*g*). Purified nanoparticles were resuspended in ultrapure water and stored at 4 °C until use.

SDS-PAGE analysis: the profile of proteins adsorbed to nanoparticle surfaces was visualized using the Mini PROTEAN TGX System (BioRad). Proteins were initially denatured (and desorbed from nanoparticles) in 2x Laemmli sample buffer supplemented with 1,4-dithiothreitol (50 mM), in a 1:1 ratio of sample (0.1 mg ml^{-1}) to buffer, for 10 min at 99 °C. Desorbed proteins were isolated from the nanoparticles via brief centrifugation, and subsequently separated on 4%–20% polyacrylamide gels in SDS running buffer as per the manufacturer's instructions. Proteins were then stained using Coomassie R-250, and whole-gel images captured on a ChemiDoc MP Imaging System (BioRad).

Protein quantification: to measure the total amount of proteins adsorbed to nanoparticle surfaces, a Bradford assay was performed. Proteins were desorbed and isolated from nanoparticles as described above (see *'SDS-PAGE analysis'*). The samples were then mixed with Bradford reagent, and the absorbance measured at 590 nm using an Infinite M200 Pro plate reader (Tecan, Switzerland). Total protein adsorption was then calculated by comparison to a standard curve.

LC–MS: in preparation for LC–MS analysis, normalized protein samples (0.1 mg ml^{-1}) were reduced and alkylated by dilution in a solution containing HEPES (pH 8.5; 100 mM), sodium deoxycholate (1%), tris(2-carboxyethyl)phosphine (5 mM), and 2-iodoacetamide (10 mM) and incubation at 95 °C for 10 min. Proteins were then digested via incubation with trypsin (0.01 mg ml^{-1} ; Promega Corporation) overnight at 37 °C. Proteolysis was stopped with the addition of 10X volume of 90% acetonitrile (ACN) and 1% trifluoroacetic acid (TFA). After removal of insoluble products by centrifugation (20 000 *x*g), digested proteins were loaded onto primed (equilibrated with 90% ACN and 1% TFA) solid phase extraction columns by centrifugation (2000 *x*g), and washed twice with 10% ACN and 0.1% TFA. Peptides were then eluted with elution buffer (NH_4OH_3, 1 M; ACN, 80%), dried, then resuspended in 2% ACN and 0.2% TFA. 1 μl of sample was then loaded in triplicate onto a Q exactive plus hybrid quadrupole-orbitrap mass spectrometer (ThermoFisher) via Acclaim PepMap 100 C18 LC columns (ThermoFisher). The resulting LC/MS data was analyzed using PEAKS Studio 8.5 (Bioinformatics Solutions Inc., Canada) and MASCOT (Matrix Science, UK) software.

Protein identification and analysis: Proteins were classified based on their: (i) MW provided by the LC–MS output; (ii) physiological function determined using the PANTHER categorization system [76] (or UniProt if unavailable via PANTHER); (iii) net charge at physiological pH 7.4 computed using Prot pi; and (iv) GRAVY score calculated using ExPASy ProtParam. Furthermore, for each identified protein, normalized spectral counts were calculated and utilized to determine the relative protein abundance (RPA) according to the equation provided:

$$\text{RPA}_k = \frac{(\text{SC}/\text{MW})_k}{\sum_i^n (\text{SC}/\text{MW})_i} \times 100.$$

In this context, RPA_k represents the RPA of the protein (*k*), while SC is the spectral count identified, and MW is the MW (kDa) of the protein *k* [77, 78]. $\sum_i^n (\text{SC}/\text{MW})_i$ is the sum of the normalized spectral counts in a sample comprising *n* proteins; $n = 20$ for all analyses except enrichment/depletion, where *n* encompasses all identified proteins [79].

Protein enrichment/Depletion analysis: RPA of the top 20 proteins in each corona–nanoparticle complex was compared to their respective RPA within the FBS source fluid. Herein, RPA in the total corona was used for analysis, as some highly abundant proteins found in the coronae were not present in the top 20 proteins identified in FBS. The $\log_2$ of the fold change of $RPA_{k(corona)}/RPA_{k(FBS)}$ was calculated to determine enrichment/depletion.

4.4. Cellular interaction studies

Tissue culture: three brain-derived cell types were used for *in vitro* assessment of cell uptake and viability: BV2 murine microglial cells; 1321N1 human astrocytes; and differentiated neuronal cells derived from the SH-SY5Y human neuroblastoma cell line. Cells were cultured in Dulbecco's Modified Eagle's Medium with 10% FBS and 1% Penicillin/Streptomycin at 37 °C and 5% CO_2, termed as standard conditions. SH-SY5Y cells received additional Ham's F-12 Nutrient Mix supplementation.

Neuronal cell differentiation: SH-SY5Y cells were differentiated with retinoic acid (RA) to mature neurons before use in experiments, using previously described protocols [80]. Briefly, media on seeded cells was replaced with fresh media enriched with 10 μM RA. This enriched media was replaced twice in the following 4 d (once every 2 d). Previous work from our group using this protocol has demonstrated development of characteristic polarized morphologies and extensive neurite arborization, as well as significant up-regulation of the neuronal marker NeuN and ∼50% higher activity of the enzyme acetylcholinesterase (a marker of mature cholinergic neurons), at day 7–10 *in vitro* [81]. An exemplar of RA-induced neuronal differentiation in the current work is provided in supplementary figure S3.

Flow cytometry: flow cytometry was employed to quantify the cellular uptake of bare and corona-coated nanoparticles, and to also evaluate their impact on cell viability. BV2, 1321N1 and differentiated SH-SY5Y cells were seeded at a density of 1.0×10^4 cells ml^{-1} and allowed to adhere overnight under normal conditions. The next day, BV2 and 1321N1 cells were switched into serum-depleted culture media (0% FBS); whereas SH-SY5Y cells were instead swapped into 1% FBS-supplemented media because they do not survive in media alone [56]. Each cell line was then co-incubated with 0.5 mg ml^{-1} or 1 mg ml^{-1} of fluorescent FITC-loaded nanoparticles (without or with coronas) for 6 h at 37 °C and 5% CO_2. Following incubation, culture supernatant was collected (see below), and the cells washed thrice in PBS to remove any non-internalized nanoparticles. Cells were then detached with trypsin, washed again, resuspended in FACS buffer (5% FBS, 5 mM EDTA in PBS), and spiked with DAPI stain (1 μg ml^{-1}). Nanoparticle internalization was subsequently determined on a BD LSR-II Flow Cytometer (BD Biosciences, USA). Cells were identified by forward- and side-scatter (FSC/SSC) and the live/dead population (i.e., viability) gated using DAPI (358 nm filter)/FSC. Nanoparticle internalization was detected by then gating FITC emission (488 nm filter). >20 000 events were recorded for all samples, and data analysis performed with FlowJo software (Version 10.9).

Fluorescent microscopy: fluorescent microscopy was used to visualize nanoparticle internalization. Cells were seeded at a density of 1.0×10^4 cells ml^{-1} under normal conditions and allowed to adhere to microscope cover slips inside the wells of a 6-well plate overnight. The following day, media was replaced with serum-depleted media as above, and cells were co-incubated with FITC-loaded nanoparticles (500 μg ml^{-1}) for 6 h. After incubation, cells were washed thoroughly and fixed (4% paraformaldehyde) at room temperature for 15 min. Cells were again washed before nuclei counterstaining with DAPI (10 μg ml^{-1}), followed by a third wash. Coverslips were then mounted on microscope slides, and nanoparticle uptake by cells visualized on a Nikon A1R confocal microscope with all images processed using NIS Elements software (Nikon).

Cytokine assays: a cytometric bead array (CBA) was used to quantify any secretion of pro-inflammatory cytokines from cells exposed to nanoparticles (with and without coronas). The concentration of TNF and IL-6 in previously obtained cell supernatants was measured with a BD Biosciences Flex Set [82]. Specifically, BV2 cell supernatant was analyzed against murine standards, while 1321N1 and SH-SY5Y cell supernatants were analyzed against human standards. All collected data was processed in BD CBA analysis software.

Statistical Analysis: Statistical significance was determined via Two-way ANOVA with Šídák, Dunnett's or Tukey's post-hoc analysis using GraphPad PRISM. Results are presented as mean ± standard deviation.

Data availability statement

All data that support the findings of this study are included within the article (and any supplementary files).

Acknowledgments

This work was supported by research grants awarded to A C and L C P from: Dementia Australia Research Foundation; Mason Foundation; and the National Foundation for Medical Research and Innovation. A C is supported by a Chancellor's Research Fellowship from the University of Technology Sydney (UTS). The authors acknowledge the technical and scientific assistance of both the UTS Proteomics, Lipidomics and Metabolomics Core Facility, and the UTS Microbial Imaging Facility. The authors also pay their respects to the Gadigal people, who are the traditional custodians of the land on which this research took place.

Supporting Information

List of Top-20 most abundant FBS proteins in nanoparticle-corona complexes after different incubation periods; functional classification of proteins identified in native FBS and nanoparticle-corona complexes; compositional analysis of coronas on nanoparticles after contact with FBS for 6 h or 12 h; protein enrichment/depletion in coronas formed

on nanoparticles after incubation with FBS for 6 or 12 h; Differentiation of SH-SH5Y cells into neurons.

Conflict of interest

The authors declare no competing financial interest.

Table of contents entry

Herein, serum-derived protein-corona coated nanoparticles are characterized, compositionally analyzed and interacted with brain cells. The corona formed on PLGA nanoparticles has greater diversity of adsorbed proteins compared to the corona formed on PLGA-PEG nanoparticles. Corona coated PLGA nanoparticles are readily internalized into microglia and neurons, while corona coated PLGA-PEG nanoparticles are not.

ORCID iDs

Nabila Morshed https://orcid.org/0000-0001-6398-616X
Claire Rennie https://orcid.org/0000-0003-4533-6627
Wei Deng https://orcid.org/0000-0002-9413-0978
Lyndsey Collins-Praino https://orcid.org/0000-0002-4380-7600
Andrew Care https://orcid.org/0000-0002-0035-7961

References

[1] Boyton I, Valenzuela S M, Collins-Praino L E and Care A 2024 *Brain Behav. Immun.* **115** 631
[2] Quader S, Kataoka K and Cabral H 2022 *Adv. Drug Deliv. Rev.* **182** 114115
[3] Zhang Z-A *et al* 2021 *J. Nanobiotechnol.* **19** 453
[4] Caracciolo G, Farokhzad O C and Mahmoudi M 2017 *Trends Biotechnol.* **35** 257
[5] Bashiri G, Padilla M S, Swingle K L, Shepherd S J, Mitchell M J and Wang K 2023 *Lab Chip* **23** 1432
[6] Rampado R, Crotti S, Caliceti P, Pucciarelli S and Agostini M 2020 *Front. Bioeng. Biotechnol.* **8** 166
[7] Mihailova L, Shalabalija D, Zimmer A, Geskovski N, Makreski P, Petrushevska M, Simonoska Crcarevska M and Glavas Dodov M 2023 *Pharmaceutics* **15** 2082
[8] Xiao W, Wang Y, Zhang H, Liu Y, Xie R, He X, Zhou Y, Liang L and Gao H 2021 *Biomaterials* **274** 120888
[9] Zhang Z *et al* 2019 *Nat. Commun.* **10** 3561
[10] Jenkins S I, Weinberg D, Al-shakli A F, Fernandes A R, Yiu H H P, Telling N D, Roach P and Chari D M 2016 *J. Control. Release* **224** 136
[11] Tang Y, Gao J, Wang T, Zhang Q, Wang A, Huang M, Yu R, Chen H and Gao X 2022 *Acta Pharm. Sin.* B **12** 2043
[12] Zhang W, Mehta A, Tong Z, Esser L and Voelcker N H 2021 *Adv. Sci.* **8** 2003937
[13] Ribovski L, Hamelmann N M and Paulusse J M J 2021 *Pharmaceutics* **13** 12
[14] Kreuter J 2014 *Adv. Drug Deliv. Rev.* **71** 2
[15] Alsaab H O *et al* 2022 *Pharmaceutics* **14** 2728
[16] Pinto M, Silva V, Barreiro S, Silva R, Remião F, Borges F and Fernandes C 2022 *Ageing Res. Rev.* **79** 101658
[17] Gulati N M, Stewart P L and Steinmetz N F 2018 *Mol. Pharm.* **15** 2900
[18] Suk J S, Xu Q, Kim N, Hanes J and Ensign L M 2016 *Adv. Drug Deliv. Rev.* **99** 28
[19] Li H, Wang Y, Tang Q, Yin D, Tang C, He E, Zou L and Peng Q 2021 *Acta Biomater.* **129** 57
[20] Berrecoso G, Crecente-Campo J and Alonso M J 2020 *Drug Deliv. Transl. Res.* **10** 730
[21] Cunha A, Gaubert A, Latxague L and Dehay B 2021 *Pharmaceutics* **13** 7
[22] Locatelli E and Comes Franchini M 2012 *J. Nanopart. Res.* **14** 1316
[23] Hersh A M, Alomari S and Tyler B M 2022 *Int. J. Mol. Sci.* **23** 8
[24] Yu Y, Luan Y and Dai W 2022 *Int. J. Biol. Macromol.* **205** 731
[25] Park S J 2020 *Int. J. Nanomed.* **15** 5783
[26] Hajipour M J, Safavi-Sohi R, Sharifi S, Mahmoud N, Ashkarran A A, Voke E, Serpooshan V, Ramezankhani M, Milani A S and Landry M P 2023 *Small* **19** 2301838
[27] Partikel K, Korte R, Mulac D, Humpf H-U and Langer K 2019 *Beilstein J. Nanotechnol.* **10** 1002
[28] Lima T, Bernfur K, Vilanova M and Cedervall T 2020 *Sci. Rep.* **10** 1129
[29] Carril M, Padro D, Del Pino P, Carrillo-Carrion C, Gallego M and Parak W J 2017 *Nat. Commun.* **8** 1542
[30] Casals E, Pfaller T, Duschl A, Oostingh G J and Puntes V 2010 *ACS Nano* **4** 3623
[31] Moore T L, Rodriguez-Lorenzo L, Hirsch V, Balog S, Urban D, Jud C, Rothen-Rutishauser B, Lattuada M and Petri-Fink A 2015 *Chem. Soc. Rev.* **44** 6287
[32] Vroman L, Adams A L, Fischer G C and Munoz P C 1980 *Blood* **55** 156
[33] Monopoli M P, Åberg C, Salvati A and Dawson K A 2012 *Nat. Nanotechnol.* **7** 779
[34] Darabi Sahneh F, Scoglio C and Riviere J 2013 *PLoS One* **8** e64690
[35] Partikel K, Korte R, Stein N C, Mulac D, Herrmann F C, Humpf H-U and Langer K 2019 *Eur. J. Pharm. Biopharm.* **141** 70
[36] Papini E, Tavano R and Mancin F 2020 *Front. Immunol.* **11** 567365
[37] Cedervall T, Lynch I, Lindman S, Berggård T, Thulin E, Nilsson H, Dawson K A and Linse S 2007 *Proc. Natl Acad. Sci. USA* **104** 2050
[38] Elliott D A, Weickert C S and Garner B 2010 *Clin. Lipidol.* **51** 555
[39] Marques C, Maroni P, Maurizi L, Jordan O and Borchard G 2024 *Int. J. Biol. Macromol.* **256** 128339
[40] Marques C, Maurizi L, Borchard G and Jordan O 2022 *Int. J. Mol. Sci.* **23** 16124
[41] Altinoz M A, Guloksuz S, Schmidt-Kastner R, Kenis G, Ince B and Rutten B P F 2019 *Exp. Gerontol.* **126** 110680
[42] Garland P *et al* 2020 *Brain Commun.* **2** 1
[43] Mekseriwattana W, Thiangtrongjit T, Reamtong O, Wongtrakoongate P and Katewongsa K P 2022 *ACS Omega* **7** 37589
[44] Liu N, Tang M and Ding J 2020 *Chemosphere* **245** 125624
[45] Garland E F, Hartnell I J and Boche D 2022 *Front. Neurosci.* **16** 824888
[46] Faber D S and Pereda A E 2018 *Front. Mol. Neurosci.* **11** 427
[47] Peng Y, Chu S, Yang Y, Zhang Z, Pang Z and Chen N 2021 *Front. Pharmacol.* **12** 671734
[48] Gurwitz D 2016 *Dialogues Clin. Neurosci.* **18** 267
[49] De Vries G H and Boullerne A I 2010 *Neurochem. Res.* **35** 1978
[50] Gatti L *et al* 2023 *Nanoscale Adv.* **5** 3749
[51] Dobrovolskaia M A, Aggarwal P, Hall J B and McNeil S E 2008 *Mol. Pharm.* **5** 487
[52] Vorselen D 2022 *Biochem. Soc. Trans.* **50** 1281

[53] Cabezas-Llobet N, Camprubí S, García B, Alberch J and Xifró X 2018 *Biochim. et Biophys. Acta* **1862** 1852
[54] Zhou T, Huang Z, Zhu X, Sun X, Liu Y, Cheng B, Li M, Liu Y, He C and Liu X 2018 *Front. Immunol.* **9** 1202
[55] Ducray A D, Stojiljkovic A, Möller A, Stoffel M H, Widmer H-R, Frenz M and Mevissen M 2017 *Nanomedicine* **13** 1195
[56] De Conto V, Cheung V, Maubon G, Souguir Z, Maubon N, Vandenhaute E and Bérézowski V 2021 *Toxicol. in vitro* **77** 105235
[57] Pandey M, Choudhury H, Abdul-Aziz A, Bhattamisra S K, Gorain B, Su J S T, Tan C L, Chin W Y and Yip K Y 2020 *Pharmaceutics* **13** 1
[58] Hsiao I-L, Hsieh Y-K, Chuang C-Y, Wang C-F and Huang Y-J 2017 *Environ. Toxicol.* **32** 1742
[59] Haase A, Rott S, Mantion A, Graf P, Plendl J, Thünemann A F, Meier W P, Taubert A, Luch A and Reiser G 2012 *Toxicol. Sci.* **126** 457
[60] Dos Santos T, Varela J, Lynch I, Salvati A and Dawson K A 2011 *PLoS One* **6** e24438
[61] Annu A S, Qamar Z, Md S, Alhakamy N A, Baboota S and Ali J 2022 *Front. Bioeng. Biotechnol.* **10** 788128
[62] Teleanu D M, Chircov C, Grumezescu A M and Teleanu R I 2019 *Nanomaterials* **9** 96
[63] Jayaraman A, Htike T T, James R, Picon C and Reynolds R 2021 *Acta Neuropathol. Commun.* **9** 159
[64] Erta M, Quintana A and Hidalgo J 2012 *Int. J. Biol. Sci.* **8** 1254
[65] Decourt B, Lahiri D K and Sabbagh M N 2017 *Curr. Alzheimer Res.* **14** 412
[66] Fu P and Peng F 2022 *PLoS One* **17** e0274503
[67] Jung Y J, Tweedie D, Scerba M T and Greig N H 2019 *Front. Cell Dev. Biol.* **7** 313
[68] Minogue A M, Barrett J P and Lynch M A 2012 *J. Neuroinflammation* **9** 126
[69] Ringheim G E, Burgher K L and Heroux J A 1995 *J. Neuroimmunol.* **63** 113
[70] Yang L, Blumbergs P C, Jones N R, Manavis J, Sarvestani G T and Ghabriel M N 2004 *Spine* **29** 966
[71] Voigt N, Henrich-Noack P, Kockentiedt S, Hintz W, Tomas J and Sabel B A 2014 *J. Nanopart. Res.* **16** 6
[72] Ramalho M J, Torres I D, Loureiro J A, Lima J and Pereira M C 2023 *ACS Appl. Nano Mater.* **6** 14191
[73] Sánchez-López E *et al* 2018 *J. Nanobiotechnol.* **16** 32
[74] Cox A *et al* 2018 *ACS Nano* **12** 7292
[75] Piacentini E 2016 *Encyclopedia of Membranes* ed E Drioli and L Giorno (Springer) pp 706
[76] Thomas P D, Campbell M J, Kejariwal A, Mi H, Karlak B, Daverman R, Diemer K, Muruganujan A and Narechania A 2003 *Genome Res.* **13** 2129
[77] Monopoli M P, Walczyk D, Campbell A, Elia G, Lynch I, Baldelli Bombelli F and Dawson K A 2011 *J. Am. Chem. Soc.* **133** 2525
[78] Pustulka S M, Ling K, Pish S L and Champion J A 2020 *ACS Appl. Mater. Interfaces* **12** 48284
[79] Strojan K, Leonardi A, Bregar V B, Križaj I, Svete J and Pavlin M 2017 *PLoS One* **12** e0169552
[80] de Medeiros L M *et al* 2019 *Mol. Neurobiol.* **56** 7355
[81] Amro Z, Collins-Praino L E and Yool A J 2024 *Biosci. Rep.* **44** 3
[82] Stevens M T, Nagaria B D, Britton W J and Saunders B M 2021 *Immunol. Cell Biol.* **99** 1085